RESEARCH ARTICLE

Recent and future trends in sea surface temperature across the Persian Gulf and Gulf of Oman

Roohollah Noori[1,2]*, **Fuqiang Tian**[2], **Ronny Berndtsson**[3], **Mahmud Reza Abbasi**[4], **Mohammadreza Vesali Naseh**[5], **Anahita Modabberi**[1], **Ali Soltani**[1], **Bjørn Kløve**[6]

1 School of Environmental, College of Engineering, University of Tehran, Tehran, Iran, **2** Department of Hydraulic Engineering, State Key Laboratory of Hydroscience and Engineering, Tsinghua University, Beijing, China, **3** Department of Water Resources Engineering & Center for Middle Eastern Studies, Lund University, Lund, Sweden, **4** National Institute of Oceanography and Atmospheric Science, Tehran, Iran, **5** Department of Civil Engineering, Faculty of Engineering, Arak University, Arak, Iran, **6** Water Resources and Environmental Engineering Research Unit, Faculty of Technology, University of Oulu, Oulu, Finland

* noor@ut.ac.ir

Abstract

Climate change's effect on sea surface temperature (SST) at the regional scale vary due to driving forces that include potential changes in ocean circulation and internal climate variability, ice cover, thermal stability, and ocean mixing layer depth. For a better understanding of future effects, it is important to analyze historical changes in SST at regional scales and test prediction techniques. In this study, the variation in SST across the Persian Gulf and Gulf of Oman (PG&GO) during the past four decades was analyzed and predicted to the end of 21st century using a proper orthogonal decomposition (POD) model. As input, daily optimum interpolation SST anomaly (DOISSTA) data, available from the National Oceanic and Atmospheric Administration of the United States, were used. Descriptive analyses and POD results demonstrated a gradually increasing trend in DOISSTA in the PG&GO over the past four decades. The spatial distribution of DOISSTA indicated: (1) that shallow parts of the Persian Gulf have experienced minimum and maximum values of DOISSTA and (2) high variability in DOISSTA in shallow parts of the Persian Gulf, including some parts of southern and northwestern coasts. Prediction of future SST using the POD model revealed the highest warming during summer in the entire PG&GO by 2100 and the lowest warming during fall and winter in the Persian Gulf and Gulf of Oman, respectively. The model indicated that monthly SST in the Persian Gulf may increase by up to 4.3 °C in August by the turn of the century. Similarly, mean annual changes in SST across the PG&GO may increase by about 2.2 °C by 2100.

Introduction

Sea surface temperature (SST) variations under climate change influence species in the marine environment and may thus threaten sensitive ocean corals, alter the intensity and frequency of

blooms, reduce the nutrient flux from the deep to surface waters, raise sea level, change the global food chain, and create health-related problems for humanity by providing a more suitable environment for pathogenic microbes [1–6]. The variations in SST can also have a significant impact on climate components [7–10]. Several studies have demonstrated that SST has increased at global scale during the 20th century [11–13], while regional studies in some parts of the world have found that shallow waters such as gulfs may display a larger variation in SST increase compared with deep water areas [14]. This may be a result of the relatively lower water depth in shallow water bodies [15–17]. Gulfs are mainly affected by their surrounding land mass and therefore the SST in such water bodies is also affected by air temperature, which consequently leads to more variability. For example, the decadal rate of SST increase in Narragansett Bay, USA, which is about 1.1 ˚C, is four times greater than that of the main ocean [18].

The Persian Gulf and Gulf of Oman (PG&GO) are important water bodies from an economic, political, environmental, and social perspective. Sea surface temperature in PG&GO has shown an increasing trend during recent decades [19–25]. However, climate change effects on SST variations are not similar in either time or space and, although reported results reveal an increasing trend in global mean SST, data on the trends at regional level are limited and sometimes inconsistent [8,26,27]. In addition, climate change effects on future trends and variations in SST will be different depending on region, due to driving forces including potential change in ocean circulation and internal climate variability, ice cover, thermal stability, and ocean mixing layer depth [28]. Therefore, far-reaching analysis at regional scale using measured SST and prediction of future SST would help authorities to mitigate harmful effects of global warming on marine ecosystems. In particular, long-term prediction of SST is important at regional scale for PG&GO, due to local effects on marine ecosystems, local climate, and beyond. Researchers have attempted to project future SST using different types of global circulation models [29–31]. However, these models are complex and consist of different components such as atmosphere, ocean, land, sea ice, chemistry, and biology [32]. This makes them data heavy and they require large amounts of measured data in order to make reliable predictions. A simpler model may be relevant when data availability is sparse.

The aim of this study was to evaluate spatiotemporal variations in SST across PG&GO, which is located in the Middle East between Iran and the Arabian Peninsula. For this purpose, variations in daily optimum interpolated SST anomaly (DOISSTA) data for PG&GO during the past four decades, which are available from the National Oceanic and Atmospheric Administration (NOAA) in the United States, were analyzed. The analysis comprised two stages. In the first stage, spatiotemporal descriptive statistics on the DOISSTA data were investigated for PG&GO. In the second stage, the proper orthogonal decomposition (POD) method was used to capture dominant modes of DOISSTA. The POD model have previously been shown to represent accurately the pattern of DOISSTA variation in the northeastern part of the Indian Ocean [33]. In addition, SST across PG&GO during the 21st century was predicted using the POD model, which learns potential future warming patterns from the past behavior of historical DOISSTA trends. The POD approach has been widely applied in the field of computational fluid dynamics, but its application has been more rarely reported in oceanic and atmospheric studies [34,35].

Study area

The Persian Gulf and Gulf of Oman, a climate change hotspot [36], borders Iran in the north, Iraq and Pakistan in the northwest and northeast, respectively, and Oman, United Arab Emirates, Qatar, Kuwait, Bahrain, and Saudi Arabia in the south (Fig 1). The water mass is connected to the Arabian Sea and ocean water in the east. The climate of surrounding land is dry
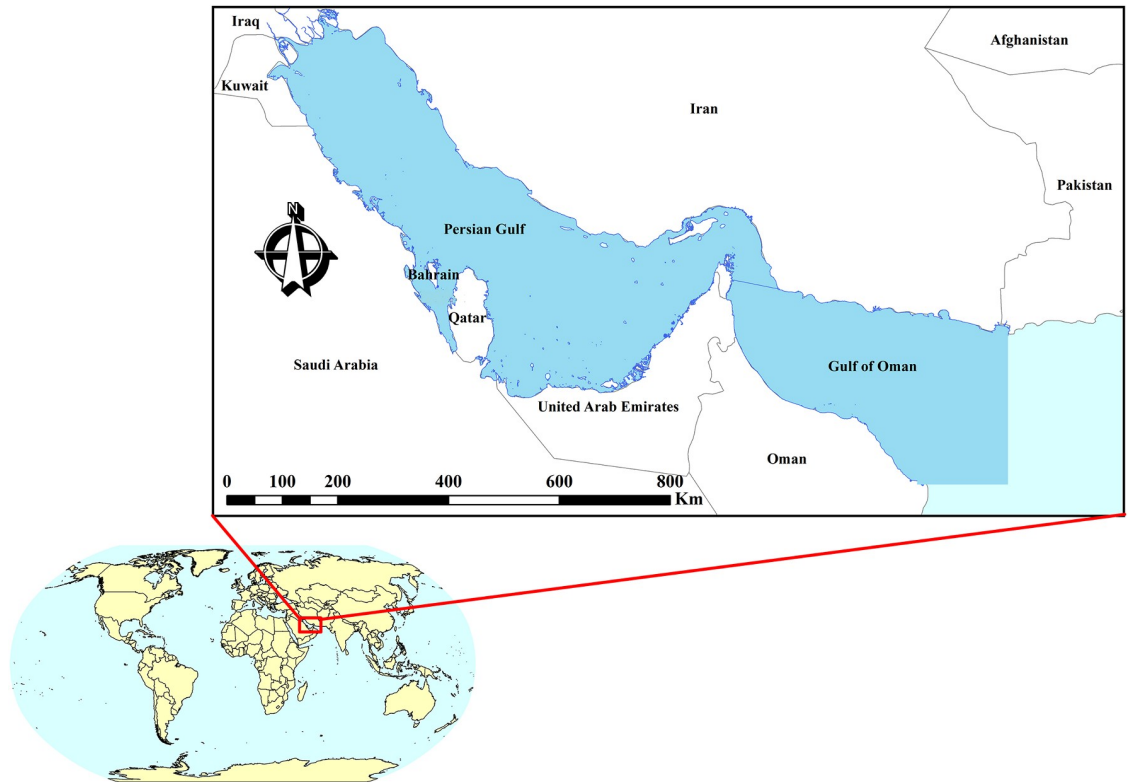
Fig 1. Map showing the study area and surrounding countries.

and subtropical. Air temperature exceeds 50 ˚C in summer and evaporation rate exceeds rainfall in PG&GO. Mean annual rainfall along the southern and northern coasts is less than 50 and 200 mm, respectively. Freshwater discharge into PG&GO is mainly provided by the rivers of Iran, among which Arvand Rud provides the largest share. On the south coast, small amounts of freshwater flow into PG&GO. Higher salinity concentration in PG&GO than in the Indian Ocean, especially in western parts including the Persian Gulf, is the main factor influencing water exchange between PG&GO and the ocean [37,38].

The study area consists of the largest and most important transportation network between Europe, Africa, and South Asia, and it includes two-thirds and one-third of the world's known oil and gas reserves, respectively [39]. Moreover, the water body is one of the largest habitats for marine organisms, such as corals, fish, and mammals [19,20,40,41]. Considering the importance of PG&GO, environmental and ecosystem protection has always been a challenge for the surrounding countries. Oil platforms and refineries around the Persian Gulf, discharge of oil, chemicals, and waste into the water, oil and gas transport in huge tankers, and outbreak of several wars in this region are the main factors threatening aquatic ecosystems of PG&GO [19]. This, together with the impact of climate change on aquatic ecosystems of PG&GO, have caused unsustainable conditions in the water body. A SST increase could exacerbate the effects of different pollution loads in PG&GO [42].

These challenges have prompted the coastal states of PG&GO to pay particular attention to this water body during implementation of national development programs, so as to protect the future sustainability of PG&GO. To assess the success of this work, this study investigated recent and future trends in SST across PG&GO.

Materials and methods

Previous studies have investigated SST variations using monthly data [43,44], while Shaltout and Omstedt [45], Hobday et al. [46], and Noori et al. [33] used daily SST data to study marine extreme temperatures. Generally speaking, the variability is higher for daily SST data than for data recorded at monthly time scales, reaching about 1.5 times higher in some parts of the ocean [28]. As monthly SST datasets are averaged from daily data, they are smoothed and do not properly show extreme high and lows of SST. Therefore, in this study we used DOISSTA data to reveal the high and low extremes of SST across PG&GO. The DOISTA data available from the NOAA website have a spatial resolution of 0.25 degree on a daily basis. The data comprise multiple sensor observations (satellites, ships, and marine buoys). More details on the DOISSTA database are presented in Reynolds et al. [47] and Reynolds [48].

The DOISSTA database covers the period from January 1982 to December 2015. The data are available in NETCDF format and can be loaded and managed by the MATLAB software. The extracted DOISSTA data for our study area resulted in 609 square 0.25 degree grids, each of which contained DOISSTA data for a total of 12,784 days. Thus, the final database was a matrix for DOISSTA containing 609 rows and 12,784 columns, as shown in Fig 2. In the matrix, rows indicate the number of grids (x_i) and columns represent the number of days (t_i).

The DOISSTA matrix data were first analyzed in terms of descriptive statistics such as mean, minimum, maximum, and standard deviation (Fig 3). In the second stage, the POD method was used to extract the dominant spatiotemporal patterns in DOISSTA for the study area (Fig 3). The POD method was independently introduced by a number of scientists, e.g., Kosambi [49], Loeve [50], Karhunen [51], Pougachev [52], and Obukhov [53]. It is a statistics-based method that extracts spatiotemporal structures of an objective parameter available from simulations or experiments [33]. In other words, POD is a linear procedure for extracting a basis for modal decomposition from an ensemble of data called "snapshots". It is noteworthy that, although the POD is a linear procedure, it is as blind as Fourier analysis and makes no assumptions on the linearity of the objective parameter [54]. However, the main advantage of POD lies in its mathematical properties, which render the method the preferred basis to use in many situations [54]. By application of the POD method, low-dimensional approximations of a high-dimensional problem can be optimally obtained. Therefore, the POD always results in a finite number of modes that properly capture the dominant features of an infinite objective problem [55].

When applying POD to the DOISSTA data, spatial and temporal components ($\Theta_i(\mathbf{x})$ and $\alpha_i(t)$, respectively) were considered according to [56,57]:

$$\mathbf{DOISSTA}(\mathbf{x}, t) = \sum_{i=1}^{N} \alpha_i(t)\Theta_i(\mathbf{x}) \tag{1}$$

In order to calculate $\Theta_i(\mathbf{x})$, it is necessary to solve Eq (2) to estimate the eigenvalues and their corresponding eigenvectors [58,59]:

$$|1 - \lambda\mathbf{I}| = 0 \tag{2}$$

where λ is the eigenvalue such that $\lambda_1 \geq \lambda_2 \geq \lambda_3 \geq \cdots \geq \lambda_N \geq 0$ and $\mathbf{I}$ is the unit matrix. Having eigenvalues and their corresponding eigenvectors, one can calculate $\Theta_i(\mathbf{x})$ using Eq (3) [60,61]:

$$\Theta_1(\mathbf{x}) = \sum_{i=1}^{N} \beta_{1i}\mathbf{DOISSTA}^{(i)}, \Theta_2(\mathbf{x}) = \sum_{i=1}^{N} \beta_{2i}\mathbf{DOISSTA}^{(i)}, \dots, \Theta_N(\mathbf{x}) = \sum_{i=1}^{N} \beta_{Ni}\mathbf{DOISSTA}^{(i)} \tag{3}$$
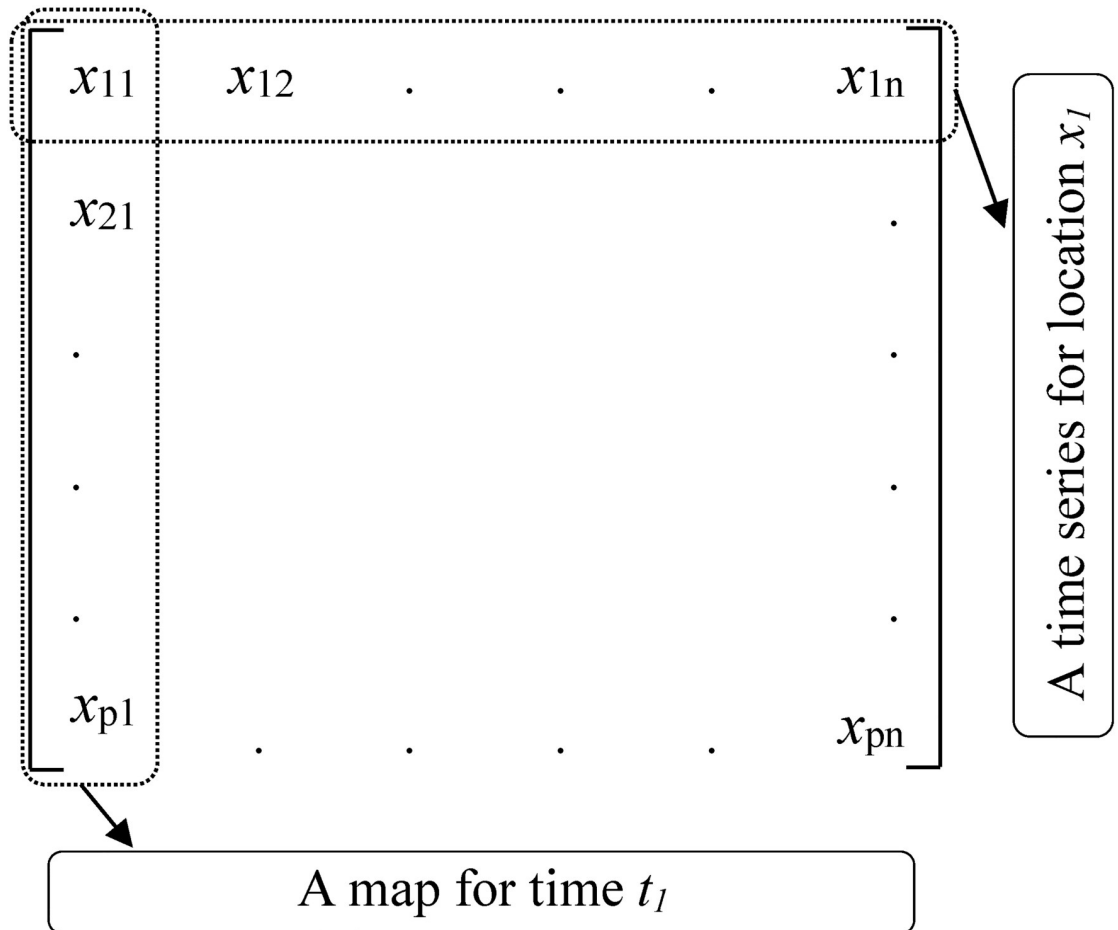
Fig 2. Prepared daily optimum interpolation SST anomaly (DOISSTA) data in matrix format.

where β_{ii} are eigenvectors corresponding to the eigenvalues. Finally, $\alpha_i(t)$ can be calculated by [62,63]:

$$\alpha(t) = (\mathbf{DOISSTA}(\mathbf{x}, t), \Theta(\mathbf{x})) \tag{4}$$

In the POD application, the first few eigenvalues are most important, as they represent the main energy in the system (here DOISSTA variations in PG&GO) [64]. Thus, by using the first few modes (K) corresponding to the first few calculated eigenvalues, it was possible to represent DOISSTA variations in PG&GO. In addition, using just the first few modes one can regenerate DOISSTA data using Eq (5) [56].

$$\mathbf{DOISSTA}(\mathbf{x}, t) \cong \sum_{i=1}^{K} \alpha_i(t)\Theta_i(\mathbf{x}) \qquad K \ll N \tag{5}$$

By considering the fact that only $\alpha_i(t)$ will change in the future, Noori et al. [33] updated Eq
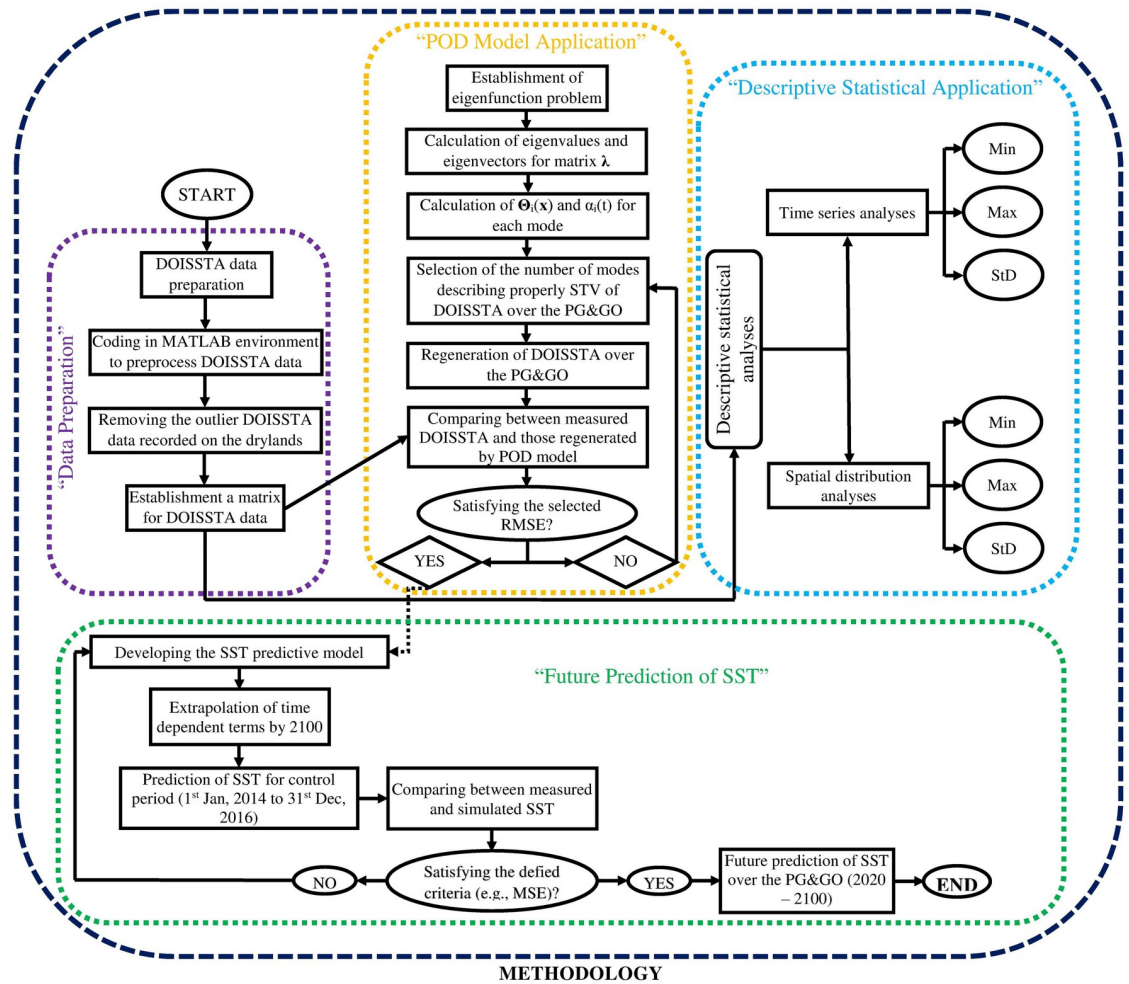
Fig 3. Schematic diagram of the analytical procedure involving the POD method used in the present study.

(5) so that it can be used for prediction as:

$$\mathbf{DOISSTA}(\mathbf{x}, t + l) \cong \sum_{i=1}^{K} \alpha_i(t + l)\Theta_i(\mathbf{x}) \qquad K \ll N \qquad (6)$$

where l is the future target time.

According to "Future Prediction of SST" in Fig 3, we extrapolated $\alpha_i(t)$ from 2016 to 2100. Thereafter, the model performance was checked by comparing predicted and measured SST data available from the NOAA website during the control period 2016–2018. Finally, SST data were estimated by application of Eq (6) for PG&GO during 2020–2100. Note that the developed POD model had a spatial and temporal resolution equal to the DOISSTA data used, i.e., 0.25 degree and one day, respectively.

The POD model predicted SST based on the assumption that it will continue to develop according to the pattern embedded in the historical records. Sanford et al. [65] report that emissions of greenhouse gases have been consistent with the representative concentration pathway 8.5 (RCP8.5) of the Fifth Assessment Report of the Intergovernmental Panel on Climate Change (IPCC) [66] from the beginning of 2005. RCP8.5 is similar to emissions scenario

A1FI used in the Fourth Assessment Report of the IPCC [67]. Therefore, the POD predictions can be expected to be comparable with those projected by global circulation models such as the Community Model Inter-comparison Project Phase 5 (CMIP5) based on RCP8.5 [68].

Results and discussion

Descriptive statistics

The mean, minimum, maximum, and standard deviation in DOISSTA for PG&GO (including 609 grids with a spatial resolution of 0.25 degree) are shown in Fig 4A–4D, respectively. As can be seen from Fig 4A–4C, there was an increase in the mean, minimum, and maximum trends of DOISSTA, corresponding to approximately 1 ˚C over 34 years. This increasing trend in DOISSTA for PG&GO confirms findings by other researchers [21–25,33]. It is worth noting that, even though the increasing trend had a low gradient, it may still be important due to the sensitive marine ecosystem in PG&GO [20,69]. For a better understanding of the variations in DOISST (i.e., not the anomalies) in the study area, mean annual DOISST was calculated for all 609 grids in the region over the 34-year period (Fig 4E). As can be seen from the diagram, there was a gradually increasing trend in mean annual DOISST over the period, with the trend being more pronounced in the beginning of the period (1982–1998) and thereafter relatively stable up to 2015. There was a "hiatus" in the period 1998–2012, due to lower warming rates in ambient air temperature compared with the average warming rate (long-term) and increasing rates of air temperature forecast by climate models [70]. Note that this remains to be confirmed, although it has been detected for both SST and air temperature [70,71]. High DOISST also occurred in 1998–1999, 2002, 2006, 2010, and 2015, years that were subjected to El Niño-Southern Oscillation (ENSO) that eventually led to unusually large DOISST. Some researchers have reported unusually strong and positive DOISST across PG&GO in 1998, 2002, 2006, and 2010, possibly as a result of the Indian Ocean Zonal Mode, which is connected to ENSO [20,22,72]. A link between positive DOISSTA in PG&GO and ENSO status in the Pacific has also reported [41].

The spatial variation in minimum, maximum, and standard deviation of DOISSTA are shown in Fig 4F–4H, respectively. A generally decreasing trend in minimum values from east to west was clearly evident in the study area (Fig 4F). In other words, the Persian Gulf, located in the western part of the study area, has experienced smaller DOISSTA than the Gulf of Oman. The minimum values of DOISSTA occurred along the southern coast of the Persian Gulf, between the Bahrain and Qatar coastlines (Gulf of Salwah), and in the northernmost areas of the Persian Gulf, where the river Arvand Rud discharges into the Persian Gulf. The northernmost areas of the Persian Gulf experienced the maximum values of DOISSTA. These areas are the shallowest parts of the Persian Gulf, where the water temperature is highly affected by the air temperature of the surrounding dry land. Furthermore, the water temperature of Arvand Rud, which differs from that of the Persian Gulf, plays a key role in the fluctuation in SST in the northernmost parts of the gulf. Similar to the minimum values, there was an increasing trend in maximum values of DOISSTA from east to west (Fig 4G). As regards the standard deviation of DOISSTA, it appeared that the majority of the Gulf of Oman experienced the smallest variation, due to its greater water depth and higher latent heat of vaporization (Fig 4H). The central parts of the Persian Gulf and locations close to the Strait of Hormuz experienced low variation in DOISSTA, due to greater water depth compared with other parts of the gulf. The southern coast and northernmost part of the Persian Gulf experienced the highest DOISSTA variations, as a result of being affected by air temperature of the surrounding dry land, shallow water depths in the region, and connections between the Arvand Rud
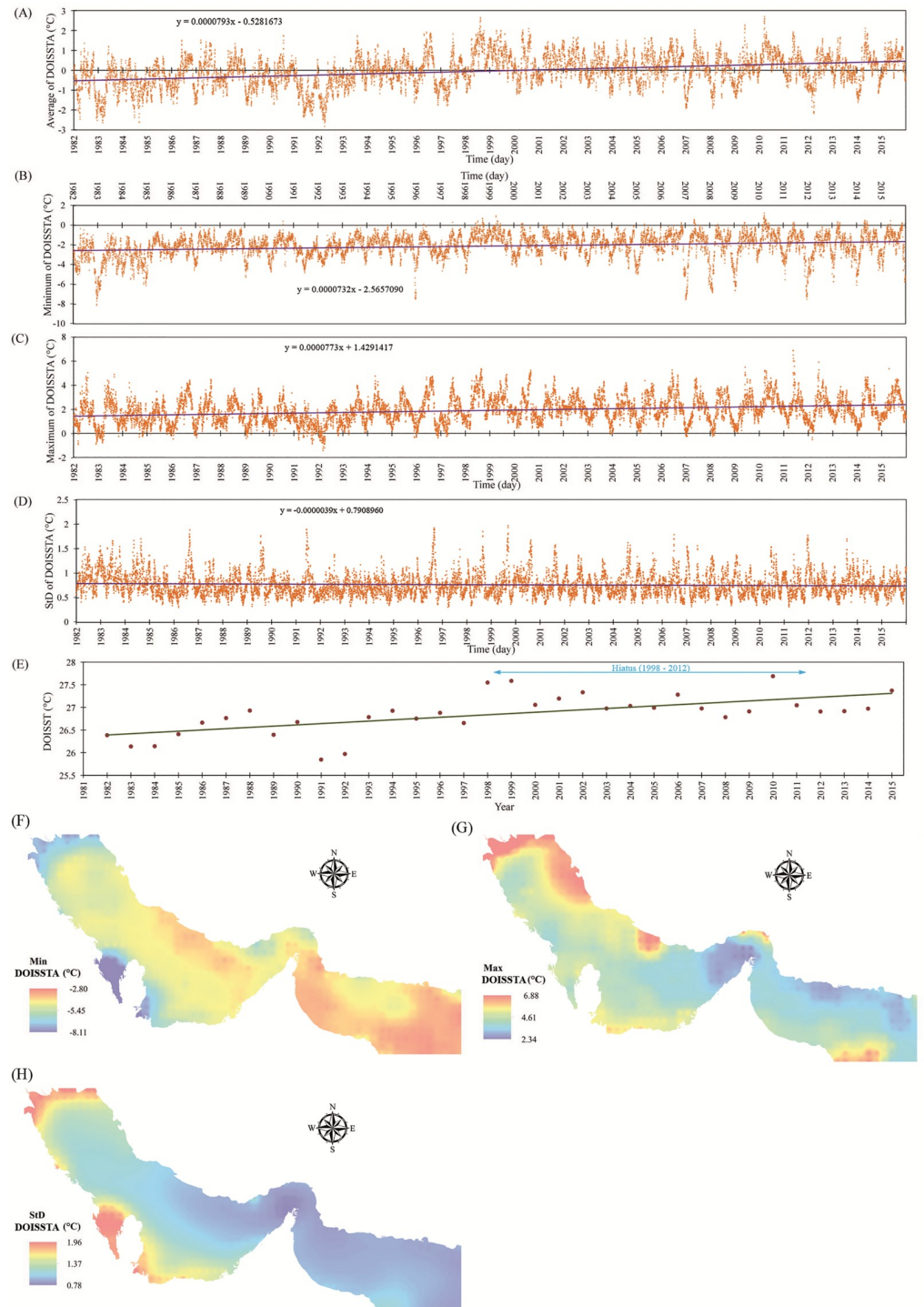
Fig 4. Historical trends in (**A**) mean values, (**B**) minimum values, (**C**) maximum values, and (**D**) standard deviation (StD) values of DOISSTA across the Persian Gulf & Gulf of Oman (PG&GO); (**E**) mean annual values of daily optimum interpolation sea surface temperature (DOISST) across PG&GO; and (**F**) spatial distribution in minimum values, (**G**) maximum values, and (**H**) standard deviation values of DOISSTA across PG&GO.

https://doi.org/10.1371/journal.pone.0212790.g004

and the Persian Gulf. These findings are comparable with results reported by Nandkeolyar et al. [22].

POD results

Mode extraction. The first 10 calculated eigenvalues, along with their conserved system energy, are shown in Fig 5. The first eigenvalue conserved about 60% of the system energy and the first five eigenvalues represented about 90% of total energy. In general, there is no a distinct formula to choose the number of modes corresponding to the eigenvalues for further investigation of an objective parameter. It is usually determined based on an energetic threshold criterion greater than 90% as used by some researchers [56,57,64]. In addition, in this study, just the first five modes have to be included as the other eigenvalues are too small to be of interest (Fig 5). Thus, using the first five modes corresponding to the first five eigenvalues, it was possible to determine the dominant pattern of DOISSTA variation in PG&GO.

The space-dependent terms for the first five modes ($\Theta_1(\mathbf{x})$ to $\Theta_5(\mathbf{x})$, respectively) are shown in Fig 6A–6E, respectively. According to the results for $\Theta_1(\mathbf{x})$, the Persian Gulf has experienced more variation in DOISSTA than the Gulf of Oman (Fig 6A). In addition, the shallow parts of PG&GO, which are mostly located along the southern coasts and northernmost parts of the Persian Gulf, showed the largest variation. Based on the results for $\Theta_1(\mathbf{x})$, the Gulf of Oman has experienced the least variation, due to its greater depth than the Persian Gulf. These findings are in line with results reported by Nandkeolyar et al. [22]. Comparing the results of $\Theta_1(\mathbf{x})$ with the spatial distribution of standard deviation calculated in the previous stage (see Fig 4H) revealed that, although the results were rather similar, there were some differences. These differences were mainly due to consideration of information from all grids in the study area for calculation of $\Theta_1(\mathbf{x})$, which leads to more realistic results [73]. For example, considering the shallower water depth in the Persian Gulf than in the Gulf of Oman, DOISSTA in the Persian Gulf can be expected to be more affected by the air temperature of surrounding dry land, which displays greater variation. Therefore, $\Theta_1(\mathbf{x})$ more accurately reflected the actual spatial variation in DOISSTA in PG&GO than the calculated standard deviation in Fig 4H. Moreover, the $\Theta_2(\mathbf{x})$ results were similar to the results for $\Theta_1(\mathbf{x})$, especially in the Persian Gulf. For example, based on the $\Theta_2(\mathbf{x})$ results, there was significant variation in DOISSTA along the southern coast and the northwestern part of the Persian Gulf during the study period (Fig 6B). In addition, the $\Theta_3(\mathbf{x})$ and $\Theta_4(\mathbf{x})$ results (shown in Fig 6C and 6D, respectively) support the results for $\Theta_1(\mathbf{x})$, with both components reflecting higher variation in southern and northernmost parts of the Persian Gulf. However, the results for $\Theta_5(\mathbf{x})$ showed little compatibility with $\Theta_1(\mathbf{x})$, as they indicated that coasts along Oman and United Arab Emirates in the Gulf of Oman experienced more variation in DOISSTA (Fig 6E).

The calculated temporal terms of all first five modes ($\alpha_1(t)$ to $\alpha_5(t)$, respectively) are shown in Fig 7A, while those for $\alpha_1(t)$ to $\alpha_5(t)$ are shown separately in Fig 7B–7F, respectively. It is worth noting that $\alpha_1(t)$ had greater importance than the other terms due to the significance of the first mode ($\Theta_1(\mathbf{x})$). As Fig 7A clearly shows, $\alpha_1(t)$ to $\alpha_5(t)$ fluctuated with an annual wavelength that matched the annual change cycle in SST. According to the results for $\alpha_1(t)$ (Fig 7B), the variation in DOISSTA was incremental and increased with a low gradient during the 34-year study period, as also reported by others [21–25,33], and the minimum DOISSTA occurred in late February each year. Thereafter, there was a warming trend, with DOISSTA reaching a maximum by the middle of August, followed by a cooling period, so that DOISSTA again reached a minimum in late February. This cycle was repeated for $\alpha_1(t)$ in each year in the study period, and is in line with reported results for SST variation in the study area [17]. Based on the high percentage of system energy conserved by the first mode, the results for
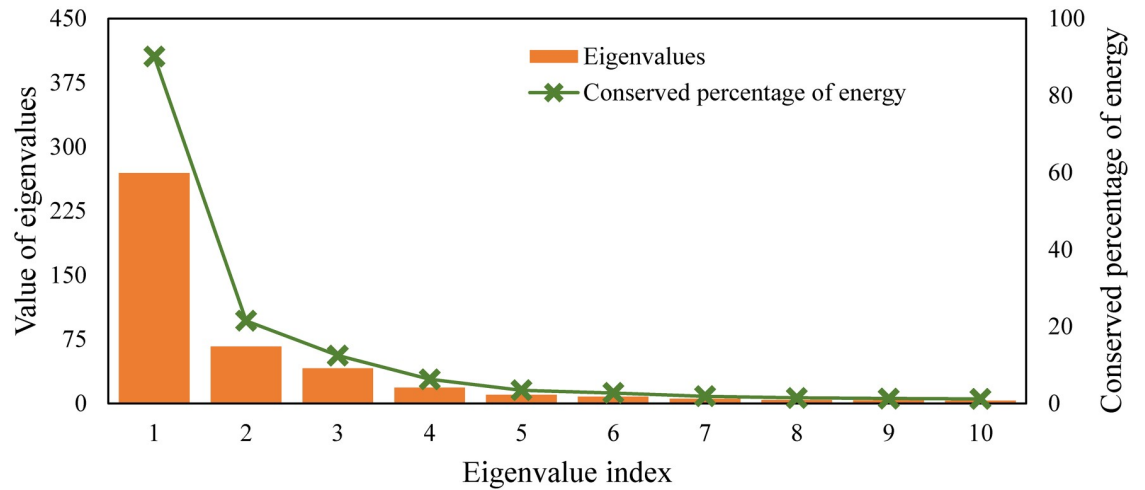
Fig 5. The first 10 calculated eigenvalues and their conserved energy percentage in the Persian Gulf & Gulf of Oman (PG&GO).

https://doi.org/10.1371/journal.pone.0212790.g005
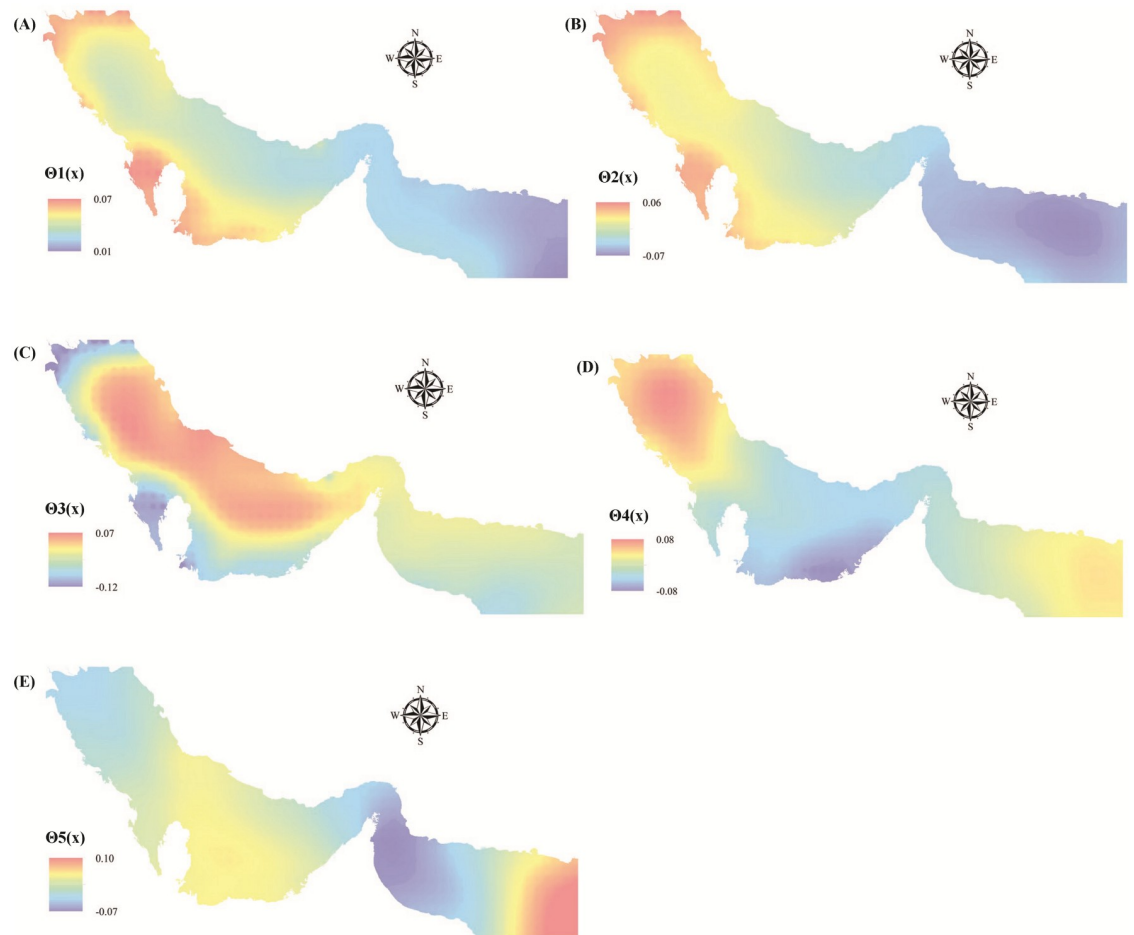
Fig 6. Pattern of space-dependent terms for (**A**) the first mode $\Theta_1(\mathbf{x})$, (**B**) the second mode $\Theta_2(\mathbf{x})$, (**C**) the third mode $\Theta_3(\mathbf{x})$, (**D**) the fourth mode $\Theta_4(\mathbf{x})$, and (**E**) the fifth mode $\Theta_5(\mathbf{x})$.

https://doi.org/10.1371/journal.pone.0212790.g006
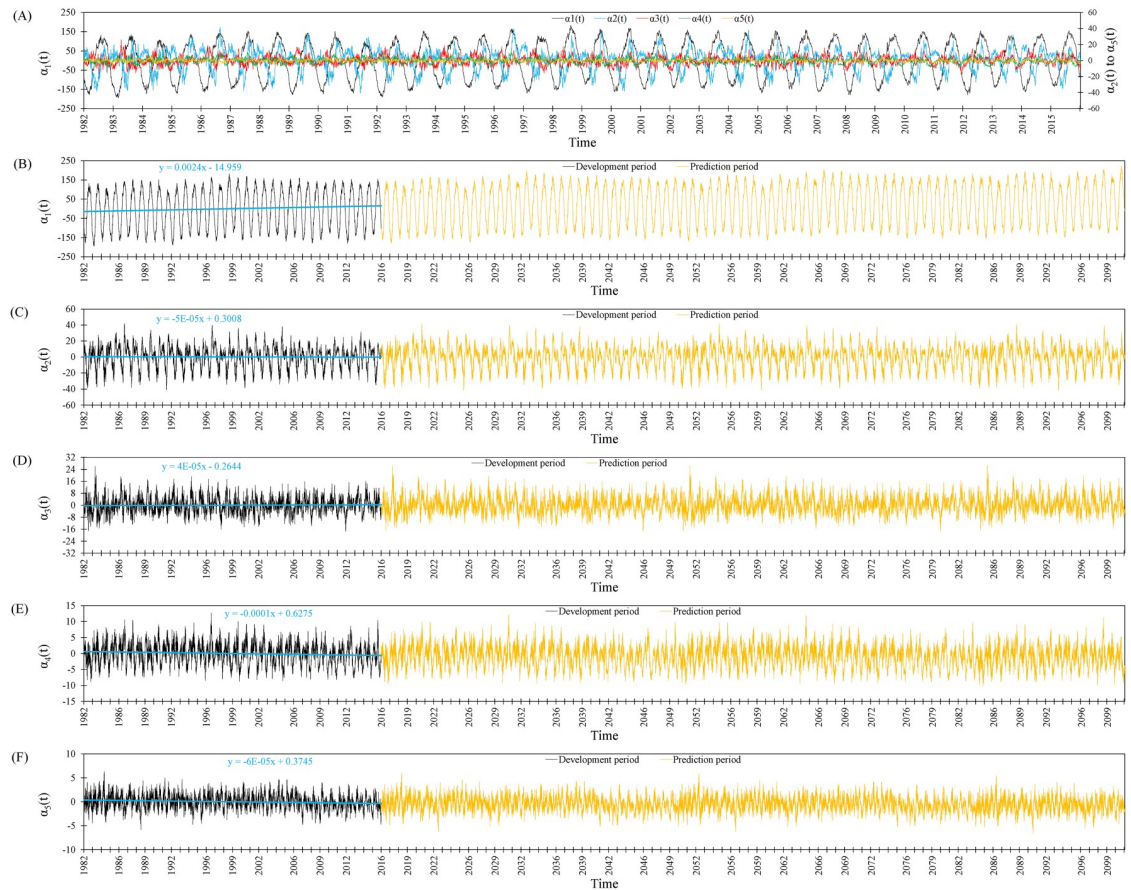
Fig 7. Pattern of time-dependent terms for (**A**) the first mode $\alpha_1(t)$, (**B**) the second mode $\alpha_2(t)$, (**C**) the third mode $\alpha_3(t)$, (**D**) the fourth mode $\alpha_4(t)$, and (**E**) the fifth mode $\alpha_5(t)$.

$\alpha_1(t)$ represented a high percentage (about 60%) of the DOISSTA variation in PG&GO. The results for $\alpha_2(t)$, $\alpha_4(t)$, and $\alpha_5(t)$ indicated a mild decreasing trend for DOISSTA (Fig 7C, 7E and 7F, respectively). These findings clearly suggest a cold bias in DOISSTA across PG&GO, which matches reported results obtained by running climate models [74]. This cold bias in DOISSTA across PG&GO regularly expands in winter and continues into spring and summer [75].

The high variation in DOISSTA across PG&GO compared with the concurrent global average may be a result of different phenomena [21]. El Niño-Southern Oscillation and the Indian Ocean Zonal Mode are undoubtedly two processes that are important drivers of DOISSTA in PG&GO. However, it has been suggested that the interplay between ENSO and the Indian Ocean Zonal Mode is not the only mechanism influencing DOISSTA in PG&GO [41]. Other investigations have indicated that a positive North Atlantic Oscillation, the Siberian high pressure system, and Shamal wind events have important effects on DOISSTA [76,77]. Furthermore, consistent warming trends for PG&GO have been reported since 1950, and especially since 1970 [78]. The air temperature over PG&GO is rapidly increasing and the increase may exceed +4 ˚C by the end of this century [79]. Furthermore, there is some evidence of a weakening influence of the Siberian high pressure system that could be a result of an increasing trend in air surface temperature over PG&GO [80]. All these results indicate that the positive rate of warming of PG&GO water could be related to the increasing trend in climate variables such as

air temperature in the study area, as well as strong effects of oceanographic events such as ENSO, the North Atlantic Oscillation, and the Indian Ocean Zonal Mode.

Model performance for control period 2016–2018. The $\alpha_1(t)$ to $\alpha_5(t)$ values for the period 2016–2100 estimated using the POD model are shown in Fig 7B to 7F, respectively (extrapolated values are shown in brown). The model performance was checked by comparing predicted and measured SST data available from the NOAA website for the control period 2016–2018. The mean absolute relative error between SST values predicted by the POD model and measured values for 2016–2018 is shown in Fig 8A. The error was less than 2% for more than 50% of days in 2016, 2017, and 2018, while it increased to about 2.7% for more than 90% of days in 2016, 2017, and 2018 (Fig 8A). Based on these results, it can be concluded that the POD model reasonably predicted SST for PG&GO.

Predictions: 2020–2100. The POD model was used to predict SST across PG&GO for the period 2020–2100. Spatial trends in mean monthly SST in February, May, August, and November (representing winter, spring, summer, and fall respectively), are illustrated in Fig 8B–8E for the selected years 2030, 2050, 2070, and 2100, respectively. The spatial distribution of mean annual SST for the selected years 2015, 2030, 2050, 2070, and 2100 is shown in Fig 9A–9E, respectively. In addition, the spatial distribution of differences between the predicted SST shown in these diagrams and those measured in 2015 are illustrated in Fig 9B–9E. All diagrams clearly show a warming trend in PG&GO in the future, and a more severe warming trend in the Persian Gulf than in the Gulf of Oman.

Based on Fig 8B–8E, summer seasons in the Persian Gulf will experience most warming by 2100, while fall seasons will experience least. Summer seasons in the Gulf of Oman will also experience most warming by 2100, while winter seasons will experience the least warming in that case. In general, the maximum difference between SST measured in 2015 and projected by the POD model was observed for the Persian Gulf, where SST was 4.3 ˚C higher by August 2100. The greatest differences for the Persian Gulf in other future years were 2.1, 2.8, and 3.4 ˚C in May 2030, May 2050, and August 2070, respectively. No previous study has projected SST for PG&GO by the end of 21st century, but the results obtained are in line with values reported for other marine environments. For example, the monthly SST projected by global circulation models under RCP8.5 indicates a rise of 4.8 and 3.7 ˚C for six large marine ecosystems of the Northwest Atlantic by the end of August and February 2100, respectively [81]. Results from 26 models in CMIP5 under scenario RCP8.5 reveal an increase of up to 6 ˚C from August 1976 to August 2099 for monthly SST over large marine ecosystems adjacent to Europe, North America, and the Arctic Ocean [28]. Additionally, SST over the Mediterranean Sea during summer and winter seasons has been estimated to rise by 2.9 and 0.5 ˚C, respectively, under scenario RCP8.5 by the end of 21st century [44].

In regards to mean annual warming, this study clearly showed that the north coast of the United Arab Emirates and south coastlines of the Strait of Hormuz will experience the highest SST in the future, reaching 32 ˚C by 2100 (Fig 9B–9E). Mean annual (maximum) SST across PG&GO may increase from 28.5 (29.9) ˚C in 2015 to 30.7 (31.8) ˚C in 2100. Such an increase would threaten natural habitats in PG&GO [82]. The increasing trend in the Mediterranean Sea is reported to about 3.1 ˚C under scenario A2 (same as A1FI, represents the highest emissions of greenhouse gases) for the period 1960–2099 [29]. The SST off the Australian coast is predicted to increase by 2–4 ˚C under RCP8.5 by 2100 [83]. Chust et al. [84] predict a positive change in SST under scenario A1B (represents moderate emissions of greenhouse gases) over the Black Sea, of around 3.7 ˚C during 2080–2100 relative to 1980–2000. The increase in annual SST for PG&GO predicted in the present study also exceeded the up to 1.3 ˚C increase in global SST during 21st century predicted by Aral and Guan [31]. In another study, the SST
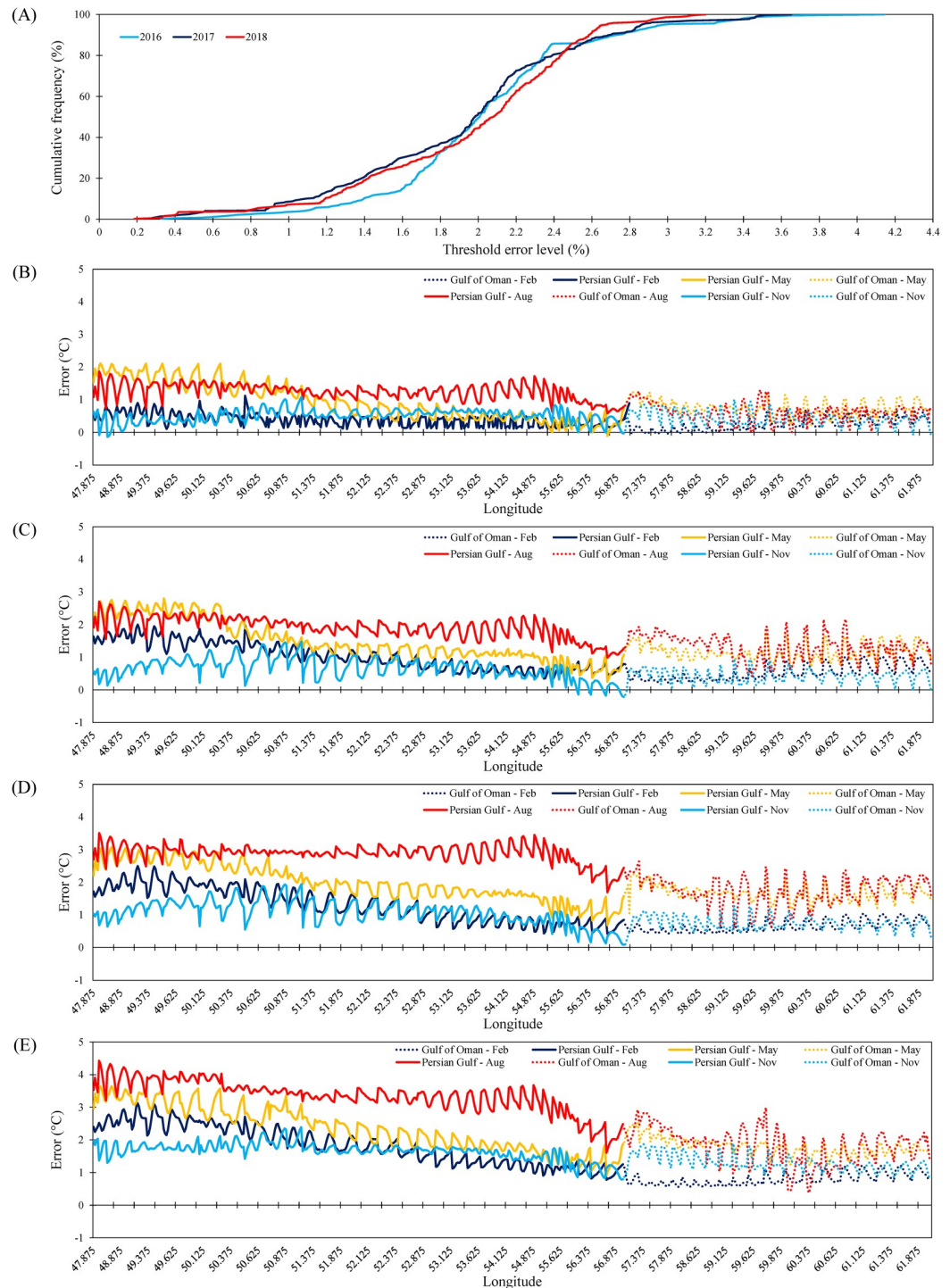
Fig 8. (**A**) Mean absolute relative error between sea surface temperature (SST) values for the Persian Gulf & Gulf of Oman (PG&GO) predicted by the proper orthogonal decomposition (POD) model and measured during the period 2016–2018; and spatial trends in mean monthly SST in (**B**) February (representing winter), (**C**) May (representing spring), (**D**) August (representing summer), and (**E**) November (representing fall) in the selected future years 2030, 2050, 2070, and 2100.
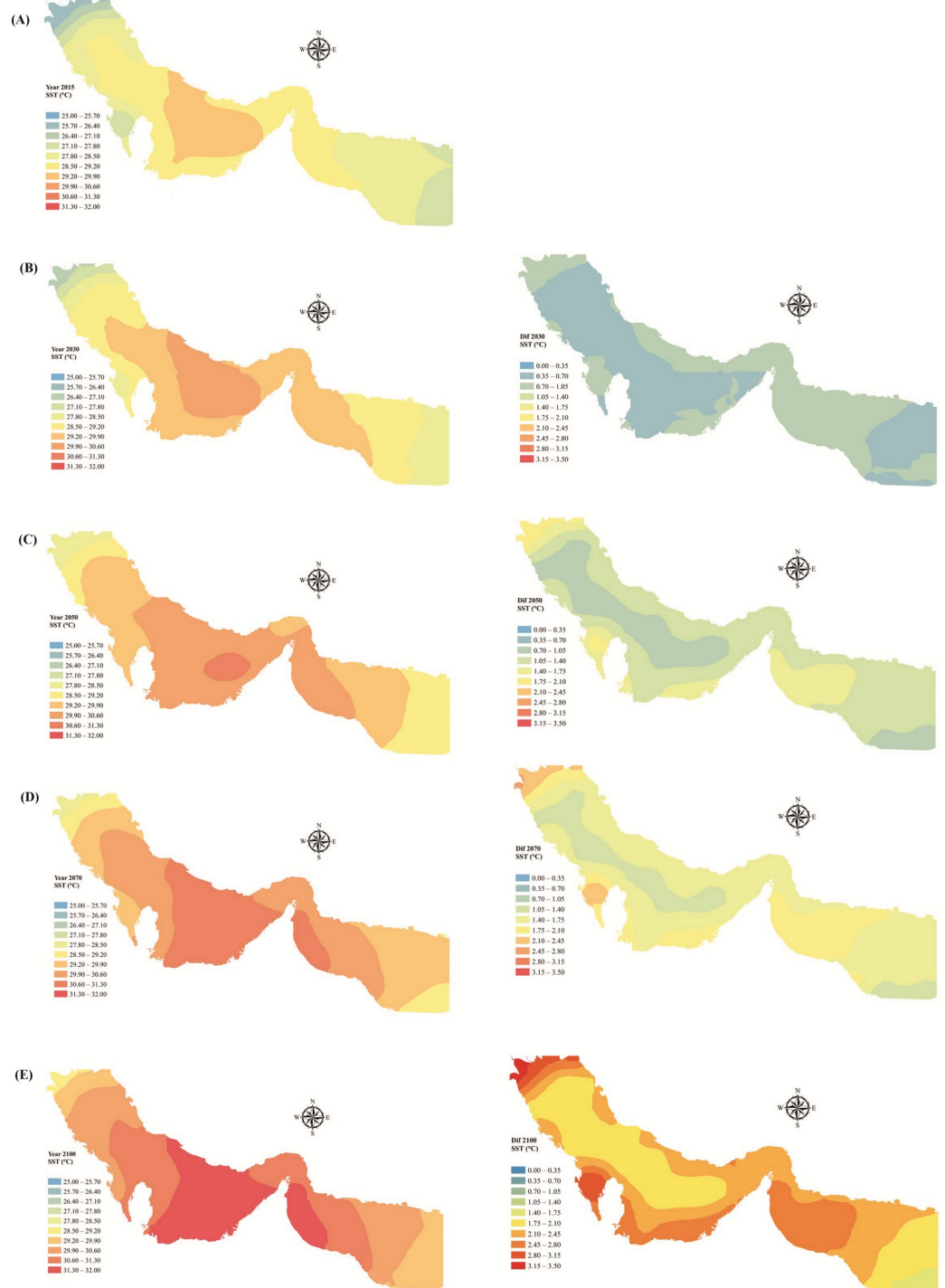
Fig 9. (**A**) Spatial distribution of mean annual sea surface temperature (SST) across the Persian Gulf & Gulf of Oman (PG&GO) for (**A**) the year 2015, (**B**) the year 2030 and difference between 2030 and 2015, (**C**) the year 2050 and difference between 2050 and 2015, (**D**) the year 2070 and difference between 2070 and 2015, and (**E**) the year 2100 and difference between 2100 and 2015.

https://doi.org/10.1371/journal.pone.0212790.g009

in the Western English Channel was predicted to increase by around 0.5 and 2.5 ˚C under scenarios RCP2.6 and RCP8.5, respectively, by the year 2100 [85].

Relative to the year 2015, our predicted monthly maximum SST warming in PG&GO by the end of 21st century is close to that estimated for large marine ecosystems and exceeds that estimated for the Mediterranean Sea. In addition, we found that summers generally showed a stronger trend than winters. This may be a result of integration of greenhouse gas warming over a much thinner climatological mixing layer depth in warm (summer) than in cold (winter) seasons, thereby intensifying the SST seasonal cycle during the 21st century [28].

Conclusions

This study evaluated variations in DOISSTA across PG&GO during the past 34 years using descriptive statistics and predicted SST by 2100 using a POD model. Investigations of DOISSTA based on statistical indices revealed an increasing trend in mean, minimum, and maximum DOISSTA of about 1 ˚C during the 34-year study period, likely due to the impacts of climate change. In the study period, the Persian Gulf experienced smaller and larger DOISSTA than the Gulf of Oman. The spatial distribution of the first mode calculated by POD revealed maximum variation in DOISSTA in the Persian Gulf, especially along its southern coasts between Bahrain and Qatar coastlines and in the northernmost area, where the river Arvand Rud discharges into the gulf.

Prediction of SST indicated that summer seasons in PG&GO will experience most warming by 2100, while the warming effect will be smaller for fall and winter seasons. The monthly maximum difference between SST measured in 2015 and SST predicted by the model for 2030, 2050, 2070, and 2100 was 2.1 (May), 2.8 (May), 3.4 (August), and (August) 4.3 ˚C, respectively. Future mean annual warming in PG&GO relative to 2015 was predicted to be highest along the north coast of the United Arab Emirates and south coastlines of the Strait of Hormuz, where SST may reach 32 ˚C by 2100. Mean annual (maximum) SST across PG&GO was predicted to increase from 28.5 (29.9) in 2015 to 30.7 (31.8) ˚C in 2100. This 2.2 ˚C increase in mean annual SST would threaten natural habitats and marine ecosystems in PG&GO.

Author Contributions

Conceptualization: Roohollah Noori.

Funding acquisition: Fuqiang Tian, Ronny Berndtsson, Bjørn Kløve.

Investigation: Fuqiang Tian.

Methodology: Roohollah Noori, Ronny Berndtsson, Mahmud Reza Abbasi.

Resources: Fuqiang Tian.

Software: Ali Soltani.

Supervision: Roohollah Noori.

Visualization: Mohammadreza Vesali Naseh, Anahita Modabberi.

Writing – original draft: Roohollah Noori, Mohammadreza Vesali Naseh, Anahita Modabberi.

Writing – review & editing: Roohollah Noori, Fuqiang Tian, Ronny Berndtsson, Bjørn Kløve.

References

1. Harvell CD, Kim K, Burkholder JM, Colwell RR, Epstei Epstein PR, Grimes DJ, et al. Emerging marine diseases—climate links and anthropogenic factors. Science. 1999; 285(5433):1505–1510. https://doi.org/10.1126/science.285.5433.1505 PMID: 10498537

2. Brander KM. Global fish production and climate change. P Natl Acad Sci USA. 2007; 104(50):19709–19714. https://doi.org/10.1073/pnas.0702059104

3. Guan J, Chang B, Aral MM. A dynamic control system model for global temperature change and sea level rise in response to CO_2 emissions. Climate Res. 2013; 58(1):55–66. https://doi.org/10.3354/cr01189

4. Ainsworth TD, Heron SF, Ortiz JC, Mumby PJ, Grech A, Ogawa D, et al. Climate change disables coral bleaching protection on the Great Barrier Reef. Science. 2016; 352(6283):338–342. https://doi.org/10.1126/science.aac7125 PMID: 27081069

5. Chang B, Guan J, Aral MM. Scientific discourse: Climate change and sea-level rise. J Hydrol Eng. 2014; 20(1):A4014003. https://doi.org/10.1061/(ASCE)HE.1943-5584.0000860

6. Gobler CJ, Doherty OM, Hattenrath-Lehmann TK, Griffith AW, Kang Y, Litaker RW. Ocean warming since 1982 has expanded the niche of toxic algal blooms in the North Atlantic and North Pacific oceans. P Natl Acad Sci USA. 2017; 114(19):4975–4980. https://doi.org/10.1073/pnas.1619575114

7. Prospero JM, Lamb PJ. African droughts and dust transport to the Caribbean: climate change implications. Science. 2003; 302(5647):1024–1027. https://doi.org/10.1126/science.1089915 PMID: 14605365

8. Trenberth KE, Dai A, Van Der Schrier G, Jones PD, Barichivich J, Briffa KR, et al. Global warming and changes in drought. Nat Clim Change. 2014; 4(1):17–22. https://doi.org/10.1038/nclimate2067

9. Ban N, Schmidli J, Schär C. Heavy precipitation in a changing climate: Does short-term summer precipitation increase faster? Geophys Res Lett. 2015; 42(4):1165–1172. https://doi.org/10.1002/2014GL062588

10. Berg N, Hall A. Increased interannual precipitation extremes over California under climate change. J Climate. 2015; 28(16):6324–6334. https://doi.org/10.1175/JCLI-D-14-00624.1

11. Cane MA, Clement AC, Kaplan A, Kushnir Y, Pozdnyakov D, Seager R, et al. Twentieth-century sea surface temperature trends. Science. 1997; 275(5302):957–960. https://doi.org/10.1126/science.275.5302.957 PMID: 9020074

12. Trenberth KE, Jones PD, Ambenje P, Bojariu R, Easterling D, Tank AK, et al. Observations: Surface and Atmospheric Climate Change. In: Solomon S, Qin D, Manning M, Chen Z, Marquis M, Averyt KB, Tignor M, Miller HL. (eds), Climate Change 2007: The Physical Science Basis. Contribution of Working Group I to the Fourth Assessment Report of the Intergovernmental Panel on Climate Change. Cambridge University Press, Cambridge, UK, 235–336; 2007.

13. Shearman RK, Lentz SJ. Long-term sea surface temperature variability along the US East Coast. J Phys Oceanogr. 2010; 40(5):1004–1017. https://doi.org/10.1175/2009JPO4300.1

14. Belkin IM. Rapid warming of Large Marine Ecosystems. Prog Oceanogr. 2009; 81(1–4):207–213. https://doi.org/10.1016/j.pocean.2009.04.011

15. Turner RE. Coastal Ecosystems of the Gulf of Mexico and Climate Change. Pages 85–103 In: Ning ZH, Turner RE, Doyle T, Abdollahi KK. (eds), Integrated Assessment of the Climate Change Impacts on the Gulf Coast Region. Gulf Coast Climate Change Assessment Council and Louisiana State University Graphic Services, Washington, D.C., USA; 2003. http://www.usgcrp.gov/usgcrp/Library/nationalassessment/gulfcoast

16. Harley CD, Randall Hughes A, Hultgren KM, Miner BG, Sorte CJ, Thornber CS, et al. The impacts of climate change in coastal marine systems. Ecol Lett. 2006; 9(2):228–241. https://doi.org/10.1111/j.1461-0248.2005.00871.x482 PMID: 16958887

17. Kämpf J, Sadrinasab M. The circulation of the Persian Gulf: a numerical study. Ocean Sci. 2006; 2(1):27–41. https://doi.org/10.5194/os-2-27-2006

18. Nixon SW, Granger S, Buckley BA. The Warming of Narragansett Bay. 41˚N 2003; 2(1):19–20. http://seagrant.gso.uri.edu/41N/Vol2No1/index.htm

19. Sheppard C, Al-Husiani M, Al-Jamali F, Al-Yamani F, Baldwin R, Bishop J, et al. The Gulf: a young sea in decline. Mar Pollut Bull. 2010; 60(1):13–38. https://doi.org/10.1016/j.marpolbul.2009.10.017 PMID: 20005533

20. Riegl B. Effects of the 1996 and 1998 positive sea-surface temperature anomalies on corals, coral diseases and fish in the Arabian Gulf (Dubai, 625 UAE). Mar Biol. 2002; 140(1):29–40. https://doi.org/10.1007/s002270100676

21. Al-Rashidi TB, El-Gamily HI, Amos CL, Rakha KA. Sea surface temperature trends in Kuwait Bay, Arabian Gulf. Nat Hazards. 2009; 50(1):73–82. https://doi.org/10.1007/s11069-008-9320-9

22. Nandkeolyar N, Raman M, Kiran GS. Comparative analysis of sea surface temperature pattern in the eastern and western gulfs of Arabian Sea and the Red Sea in recent past using satellite data. Int J Oceanogr. 2013; 2013. https://doi.org/10.1155/2013/501602

23. Moradi M, Kabiri K. Spatio-temporal variability of SST and Chlorophyll-a from MODIS data in the Persian Gulf. Mar Pollut Bull. 2015; 98(1–2):14–25. https://doi.org/10.1016/j.marpolbul.2015.07.018 PMID: 26187398

24. Shirvani A, Nazemosadat MJ, Kahya E. Analyses of the Persian Gulf sea surface temperature: prediction and detection of climate change signals. Arab J Geosci. 2015; 8(4):2121–2130. https://doi.org/10.1007/s12517-014-1278-1

25. Shirvani A. Change point detection of the Persian Gulf sea surface temperature. Theor Appl Climatol. 2017; 127(1–2):123–127. https://doi.org/10.1007/s00704-015-1625-5

26. Falvey M, Garreaud RD. Regional cooling in a warming world: Recent temperature trends in the southeast Pacific and along the west coast of subtropical South America (1979–2006). J Geophys Res Atmos. 2009; 114(D4). https://doi.org/10.1029/2008JD010519

27. Lluch-Cota SE, Tripp-Valdéz M, Lluch-Cota DB, Lluch-Belda D, Verbesselt J, Herrera-Cervantes H, et al. Recent trends in sea surface temperature off Mexico. Atmósfera. 2013; 26(4):537–546. https://doi.org/10.1016/S0187-6236(13)71094-4

28. Alexander MA, Scott JD, Friedland KD, Mills KE, Nye JA, Pershing AJ, et al. Projected sea surface temperatures over the 21st century: Changes in the mean, variability and extremes for large marine ecosystem regions of Northern Oceans. Elementa-Sci Antrop. 2018; 6(1):9. https://doi.org/10.1525/elementa.191

29. Somot S, Sevault F, Déqué M. Transient climate change scenario simulation of the Mediterranean Sea for the twenty-first century using a high-resolution ocean circulation model. Clim Dynam. 2006; 27(7–8):851–879. https://doi.org/10.1007/s00382-006-0167-z

30. Parry M, Canziani O, Palutikof J, Linden P, Hanson C. Contribution of Working Group II to the Fourth Assessment Report of the Intergovernmental Panel on Climate Change. Cambridge University Press, Cambridge, New York; 2007.

31. Aral MM, Guan J. Global sea surface temperature and sea level rise estimation with optimal historical time lag data. Water. 2016; 8(11): 519. https://doi.org/10.3390/w8110519

32. Meehl GA, Covey C, Taylor KE, Delworth T, Stouffer RJ, Latif M, et al. The WCRP CMIP3 multimodel dataset: A new era in climate change research. Bull Amer Meteor Soc. 2007; 88(9):1383–1394. https://doi.org/10.1175/BAMS-88-9-1383

33. Noori R, Abbasi MR, Adamowski JF, Dehghani M. A simple mathematical model to predict sea surface temperature over northwest Indian Ocean. Estuar Coast Shelf S. 2017; 197:236–243. https://doi.org/10.1016/j.ecss.2017.08.022

34. Ahlman D, Söderlund F, Jackson J, Kurdila A, Shyy W. Proper orthogonal decomposition for time-dependent lid-driven cavity flows. Numer Heat Tr Part-B Fund. 2002; 42(4):285–306. https://doi.org/10.1080/10407790190053950

35. Willcox K. Unsteady flow sensing and estimation via the gappy proper orthogonal decomposition. Comput Fluid. 2006; 35(2):208–226. https://doi.org/10.1016/j.compfluid.2004.11.006

36. Pal JS, Eltahir EA. Future temperature in southwest Asia projected to exceed a threshold for human adaptability. Nat Clim Change. 2016; 6(2):197–200. https://doi.org/10.1038/nclimate2833

37. Sadrinasab M, Kämpf J. Three- dimensional flushing times of the Persian Gulf. Geophys Res Lett. 2004; 31(24):L24301. https://doi.org/10.1029/2004GL020425

38. Hassanzadeh S, Hosseinibalam F, Rezaei-Latifi A. Three-dimensional numerical modeling of the water exchange between the Persian Gulf and the Gulf of Oman through the Strait of Hormuz. Oceanol Hydrobiol Stud. 2012; 41(1):85–98. https://doi.org/10.2478/s13545-012-0010-6

39. Xue P, Eltahir EA. Estimation of the heat and water budgets of the Persian (Arabian) Gulf using a regional climate model. J Climate. 2015; 28(13):5041–5062. https://doi.org/10.1175/JCLI-D-14-00189.1

40. Al-Muzaini S, Jacob PG. Marine plants of the Arabian Gulf. Environ Int. 1996; 22(3):369–376. https://doi.org/10.1016/0160-4120(96)00023-2

41. Purkis SJ, Riegl B. Spatial and temporal dynamics of Arabian Gulf coral assemblages quantified from remote-sensing and in situ monitoring data. Mar Ecol Prog Ser. 2005; 287:99–113. https://doi.org/10.3354/meps287099

42. Schiedek D, Sundelin B, Readman JWR, MacDonald RW. Interactions between climate change and contaminants. Mar Pollut Bull. 2007; 54:1845–1856. https://doi.org/10.1016/j.marpolbul.2007.09.020 PMID: 17963794

43. Bond NA, Cronin MF, Freeland H, Mantua N. Causes and impacts of the 2014 warm anomaly in the NE Pacific. Geophys Res Lett. 2015; 42(9):3414–3420. https://doi.org/10.1002/2015GL063306

44. Scannell HA, Pershing AJ, Alexander MA, Thomas AC, Mills KE. Frequency of marine heatwaves in the North Atlantic and North Pacific since 1950. Geophys Res Lett. 2016; 43(5):2069–2076. https://doi.org/10.1002/2015GL067308

45. Shaltout M, Omstedt A. Recent sea surface temperature trends and future scenarios for the Mediterranean Sea. Oceanologia. 2014; 56(3):411–443. https://doi.org/10.5697/oc.56-3.411

46. Hobday AJ, Alexander LV, Perkin SE, Smale DA, Straub SC, Oliver EC, et al. A hierarchical approach to defining marine heatwaves. Prog Oceanogr. 2016; 141:227–238. https://doi.org/10.1016/j.pocean.2015.12.014

47. Reynolds RW, Smith TM, Liu C, Chelton DB, Casey KS, Schlax MG. Daily high-resolution-blended analyses for sea surface temperature. J Climate. 2007; 20(22):5743–5496. https://doi.org/10.1175/2007JCLI1824.1

48. Reynolds RW. What's New in Version 2. OISST Web Page, NOAA/NCDC; 2009. www.ncdc.noaa.gov/sst/papers/oisst_daily_v02r00_version2-features.pdf

49. Kosambi DD. Statistics in function space. J Indian Math Soc. 1943; 7:76–88. https://doi.org/10.18311/jims/1943/17156

50. Loeve M. Sur le fonctions alatoire de second ordre. Rev Sci. 1946; 84:195–206.

51. Karhunen K. Zur spektral theorie stochasticher prozesse. Ann Acad Sci Fennicae AI. 1946; 34:1–7.

52. Pugachev VS. The general theory of correlation of random functions. Izv Akud Nauk SSSR Set Mat. 1953 17(5):401–420. http://www.mathnet.ru/links/4ac02c34eb336e1a9b7fc4576c37beb1/im3477.pdf

53. Obukbov AM. Statistical description of continuous fields. Tr Geophys Int Akad Nauk SSSR. 1954; 24 (4):3–42.

54. Berkooz G, Holmes P, Lumley JL. The proper orthogonal decomposition in the analysis of turbulent flows. Annu Rev Fluid Mech. 1993; 25(1):539–575. https://doi.org/10.1146/annurev.fl.25.010193.002543

55. Chatterjee A. An introduction to the proper orthogonal decomposition. Curr Sci. 2000; 78(7):808–817.

56. Ashrafi K. Determining of spatial distribution patterns and temporal trends of an air pollutant using proper orthogonal decomposition basis functions. Atmos Environ. 2012; 47:468–476. https://doi.org/10.1016/j.atmosenv.2011.10.016

57. Kheirabadi H, Noori R, Samani J, Adamowski JF, Ranjbar MH, Zaker NH. A reduced-order model for the regeneration of surface currents in Gorgan Bay, Iran. J Hydroinform. 2018; 20(6):1419–1435 https://doi.org/10.2166/hydro.2018.149

58. Chen H, Reuss DL, Sick V. On the use and interpretation of proper orthogonal decomposition of in-cylinder engine flows. Meas Sci Technol. 2012; 23(8):085302. https://doi.org/10.1088/0957-0233/23/8/085302

59. Noori R, Yeh HD, Ashrafi K, Rezazadeh N, Bateni SM, Karbassi A, et al. A reduced-order based CE-QUAL-W2 model for simulation of nitrate concentration in dam reservoirs. J Hydrol. 2015; 530:645–656. https://doi.org/10.1016/j.jhydrol.2015.10.022

60. Chen H, Hung DLS, Xu M, Zhuang H, Jang J. Proper orthogonal decomposition analysis of fuel spray structure variation in a spark-ignition direct-injection optical engine. Exp Fluids. 2014; 55(4):1703. https://doi.org/10.1007/s00348-014-1703-y

61. Noori R, Asadi N, Deng Z. A simple model for simulation of reservoir stratification. J Hydraul Res. 2018. https://doi.org/10.1080/00221686.2018.1499052

62. Liang YC, Lee HP, Lim SP, Lin WZ, Lee KH, Wu CG. Proper orthogonal decomposition and its applications-part I: theory. J Soun Vib. 2002; 252(3):527–544, https://doi.org/10.1006/jsvi.2001.4041

63. Chen H, Hung DLS, Xu M, Zhuang H. Cycle-to-cycle variation analysis of early flame propagation in engine cylinder using proper orthogonal decomposition. Exp Therm Fluid Sci. 2014; 58:48–55. https://doi.org/10.1016/j.expthermflusci.2014.06.017

64. Esfahanian V, Ashrafi K. Equation-Free/Galerkin-Free reduced-order modeling of the shallow water equations based on proper orthogonal decomposition. J Fluid Eng. 2009; 131(7):112–125. https://doi.org/10.1115/1.3153368

65. Sanford T, Frumhoff PC, Luers A, Gulledge J. The climate policy narrative for a dangerously warming world. Nat Clim Change. 2014; 4(3):164. https://doi.org/10.1038/nclimate2148

66. IPCC. Summary for Policymakers. In: Climate Change 2013, The Physical Science Basis. Contribution of Working Group I to the Fifth Assessment Report of the Intergovernmental Panel on Climate Change. Stocker TF, Qin D, Plattner GK, Tignor M, Allen SK, Boschung J, Nauels A, Xia Y, Bex V, Midgley PM. (eds), Cambridge University Press, Cambridge, United Kingdom and New York, NY, USA; 2007.

67. Rogelj J, Meinshausen M, Knutti R. Global warming under old and new scenarios using IPCC climate sensitivity range estimates. Nat Clim Change. 2012; 2(4):248–530. https://doi.org/0.1038/NCLIMATE1385

68. Taylor KE, Stouffer RJ, Meehl GA. An overview of CMIP5 and the experiment design. Bull Amer Meteor Soc. 2012; 93(4):485–498. https://doi.org/10.1175/BAMS-D-11-00094.1

69. Stenseth NC, Mysterud A, Ottersen G, Hurrell JW, Chan KS, Lima M. Ecological effects of climate fluctuations. Science. 2002; 297(5585):1292–1296. https://doi.org/10.1126/science.1071281 PMID: 12193777

70. Medhaug I, Stolpe MB, Fischer EM, Knutti R. Reconciling controversies about the "global warming hiatus". Nature. 2017; 545:41–47. https://doi.org/10.1038/nature22315 PMID: 28470193

71. Hausfather Z, Cowtan K, Clarke DC, Jacobs P, Richardson M, Rohde R. Assessing recent warming using instrumentally homogeneous sea surface temperature records. Sci Adv. 2017; 3(1):pe1601207. https://doi.org/10.1126/sciadv.1601207

72. Loschnigg J, Meehl GA, Webster PJ, Arblaster JM, Compo GP. The Asian monsoon, the tropospheric biennial oscillation, and the Indian Ocean zonal mode in the NCAR CSM. J Climate. 2003; 16 (11):1617–1642. https://doi.org/10.1175/1520-0442(2003)0162.0.CO;2

73. Deser C, Alexander MA, Xie SP, Phillips AS. Sea surface temperature variability: patterns and mechanisms. Annu Rev Mar Sci. 2010; 2:115–143. https://doi.org/10.1146/annurev-marine-120408-151453

74. Sandeep S, Ajayamohan RS. Origin of cold bias over the Arabian Sea in climate models. Sci Rep. 2014; 4: 6403. https://doi.org/10.1038/srep06403 PMID: 25228235

75. Levine RC, Turner AG, Marathayil D, Martin GM. The role of northern Arabian Sea surface temperature biases in CMIP5 model simulations and future projections of Indian summer monsoon rainfall. Clim Dynam. 2013; 41(1):155–172. https://doi.org/10.1007/s00382-012-1656-x

76. Shinoda T, Hendon HH, Alexander MA. Surface and subsurface dipole variability in the Indian Ocean and its relation with ENSO. Deep-Sea Res PT I. 2004; 51(5):619–635. https://doi.org/10.1016/j.dsr.2004.01.005

77. Al-Senafi F, Anis A. Shamals and climate variability in the Northern Arabian/Persian Gulf from 1973 to 2012. Int J Climatol. 2015; 35(15):4509–4528. https://doi.org/10.1002/joc.4302

78. Donat MG, Peterson TC, Brune M. Changes in extreme temperature and precipitation in the Arab region: long-term trends and variability related to ENSO and NAO. Int J Climatol. 2014; 34(9):581–592. https://doi.org/10.1002/joc.3707

79. Meehl GA, Stocker TF, Collins WD. Global Climate Projections. In: Solomon S, Qin D, Manning M et al (eds), Climate Change 2007: The Physical Science Basis. Contribution of Working Group I to the Fourth Assessment Report of the Intergovernmental Panel on Climate Change, pp: 80–87, Cambridge University Press, New York, NY, USA; 2007.

80. Piontkovski SA, Al-Gheilani HM, Jupp BP, Al-Azri AR, Al-Hashmi KA. Interannual changes in the Sea of Oman ecosystem. Open Mar Biol J. 2012; 6:38–52.

81. Khan AH, Levac E, Chmura GL. Future sea surface temperatures in Large Marine Ecosystems of the Northwest Atlantic. ICES J Mar Sci. 2013; 70(5): 915–921. https://doi.org/10.1093/icesjms/fst002

82. Ateweberhan M, McClanahan TR. Relationship between historical sea-surface temperature variability and climate change-induced coral mortality in the western Indian Ocean. Mar Pollut Bull. 2010; 60 (7):964–970. https://doi.org/10.1016/j.marpolbul.2010.03.033 PMID: 20447661

83. Poloczanska E, Hobday A, Richardson A, Anthony K, Arnould J, Beardall J, et al. Marine Climate Change in Australia: Impacts and Adaptation Responses. 2012 Report Card; 2012.

84. Chust G, Allen JI, Bopp L, Schrum C, Holt J, Tsiaras K, et al. Biomass changes and trophic amplification of plankton in a warmer ocean. Global Change Biol. 2014; 20(7):2124–2139. https://doi.org/10.1111/gcb.12562

85. L'Hévéder B, Speich S, Ragueneau O, Gohin F, Bryère P. Observed and projected sea surface temperature seasonal changes in the Western English Channel from satellite data and CMIP5 multi-model ensemble. Int J Climatol. 2017; 37(6):2831–2849. https://doi.org/10.1002/joc.4882